Supplementary Material and Methods

Fly stocks and genetics: The following lines were used in this work.

DE-Cadherin::GFP knock-in allele (Huang et al., 2009)

DE-Cadherin::mTomato (Huang et al, 2009)

ubi-DE-Cadherin::GFP (Oda and Tsukita, 2001)

zipperCPTI00297 (Kyoto Stock Centre)

sqh-Rok^{K116A}::GFP (a gift from Jennifer Zallen)

UAS-Mbs::GFP (Sen et al., 2012)

zipperCPTI00297/CyO; sqh-Rok^{K116A}::GFP/TM6B (this work)

sqh^{1}FRT101/FM7,GFP; P[w+ sqh-TS::GFP]attP1/CyO (from (Vasquez et al., 2014))

sqh^{1}FRT101/FM7,GFP; P[w+ sqh-TA::GFP]attP1/CyO (from (Vasquez et al., 2014))

sqh^{1}FRT101/FM7,GFP; P[w+ sqh-AE::GFP]attP1/CyO (from (Vasquez et al., 2014))

sqh^{1}FRT101/FM7,GFP; P[sqh-A21], DE-Cadherin::GFP/CyO (from (Jordan and Karess, 1997) and this work)

sqh^{1}FRT101/FM7,GFP; P[sqh-E21], DE-Cadherin::GFP/CyO (from (Jordan and Karess, 1997) and this work)

FRT80 *mbs*^{541}/TM6B (Lee and Treisman, 2004)

w; DE-Cadherin::GFP; FRT80 *mbs*^{541}/TM3Sb, GFP (this work)

w; DE-Cadherin::mTomato, sqh-TS::GFP; FRT80 *mbs*^{541}/TM3Sb, GFP (this work)

w; ubi-DE-Cadherin::GFP; FRT80 *mbs*^{541}/TM3Sb, GFP (this work)

c381-GAL4 (Bloomington Stock Centre)

c381-GAL4, DE-Cadherin::GFP (this work)

c381-GAL4, DE-Cadherin::mTomato (this work)

UAS-MbsN300, a constitutive active form of the Myosin Binding Subunit of Myosin Light Chain Phosphatase (Lee and Treisman, 2004)

w; c381-GAL4, DE-Cadherin::mTomato/CyO; FRT80 *mbs*^{T541}/TM3Sb, GFP (this work)

w; FRT80 *mbs*^{541}, UAS-Moe^{T599A}/TAG (from (Speck et al., 2003) and this work)

w; FRT80 *mbs*^{541}, UAS-Moe^{T599D}/TAG (from (Speck et al., 2003) and this work)

rok^{2}, FRT19A; matGal4 and *ovo*^{D1}, FRT19A/Y; hsFLP, UASRok::Venus (from Adam Martin lab).

Image analysis: The confocal z-stacks were filtered to reduce noise (median and highpass filters) and segmented in 'oTracks' as described previously. Automatic tracking identified the majority of well - imaged cells. Occasional misidentification was corrected manually in some movies by deleting mistracked cell membranes and by adding unidentified ones. Filters were also used to remove mistracked cells based on their absolute size or their change in size (very small or large cells were excluded, as were those that changed drastically in size from one frame to the next), their speed of movement from one frame to the next (in order to remove cells that are incorrectly linked in time), and the number of frames for which each cell exists. Threshold values used for filtering were determined for each movie, choosing those values which excluded the majority of mistracked cells, but preserved as many well tracked cells as possible. Incomplete cells at the edge of the embryo were also removed prior to analysis. Selected cells were then used to extract data on the apical cell surface area, cell perimeter and cell shape fluctuations. For cell perimeter measurements, pixelation artifacts were removed by smoothing the total pixelated cell perimeter without removing real cell shape. Cell shape fluctuations were analysed as described in (Blanchard et al., 2010). Note that cell shape fluctuations were analysed using the cell radius time series of individual cells, because we considered actomyosin contraction to be a radial process. The amplitude of oscillations is expressed as a percentage of apical cell radius as in Blanchard et al, 2010. Combinations of long amplitudes and long cycle lengths were the signature of time periods when there were no discernible fluctuations; we used cell radius fluctuation proportional amplitude divided by cycle length as a measure of fluctuation strength. Below a fluctuation strength threshold of 0.02, fluctuations were considered as invalid. We set a system of antero-posterior coordinates in which 0 corresponds to the centre of the AS, negative values (in µm) correspond to the anterior half of the AS and positive values correspond to the posterior half of the tissue. Embryo staging was done first within each genotype, according to the evolution of two stereotypical parameters: cell area and cell elongation, a parameter measuring both the degree of cell shape anisotropy and the orientation of the anisotropy, with positive indicating elongation in the medio-lateral direction. Time 0 corresponds to the onset of net tissue contraction in the wild-type condition. Inter-genotype aligning was done comparing the position of the posterior spiracles and the shape of the anterior and posterior canthi.

Statistics: We estimated the p-value associated with a fixed effect of differences between genotypes, allowing for random effects contributed by differences between embryos within a given genotype, calculated at each time point. Ribbons are drawn for the whole span of analysis for wild type embryos and for mutant embryos. The mean trends and ribbon width are calculated from data averaged to reduce noise (box averages of eleven-fifteen bins along the abscissa were used). The widths of ribbons straddling mean trends represent a standard error calculated from the sums of within-experiment variance and between experiment variance. To test where mutant embryos were significantly different ($p < 0.05$) from wild type, mixed-model was applied, with embryo as the random variable. The regions where $p < 0.05$ are depicted with a grey-shaded box.

Supplementary figures

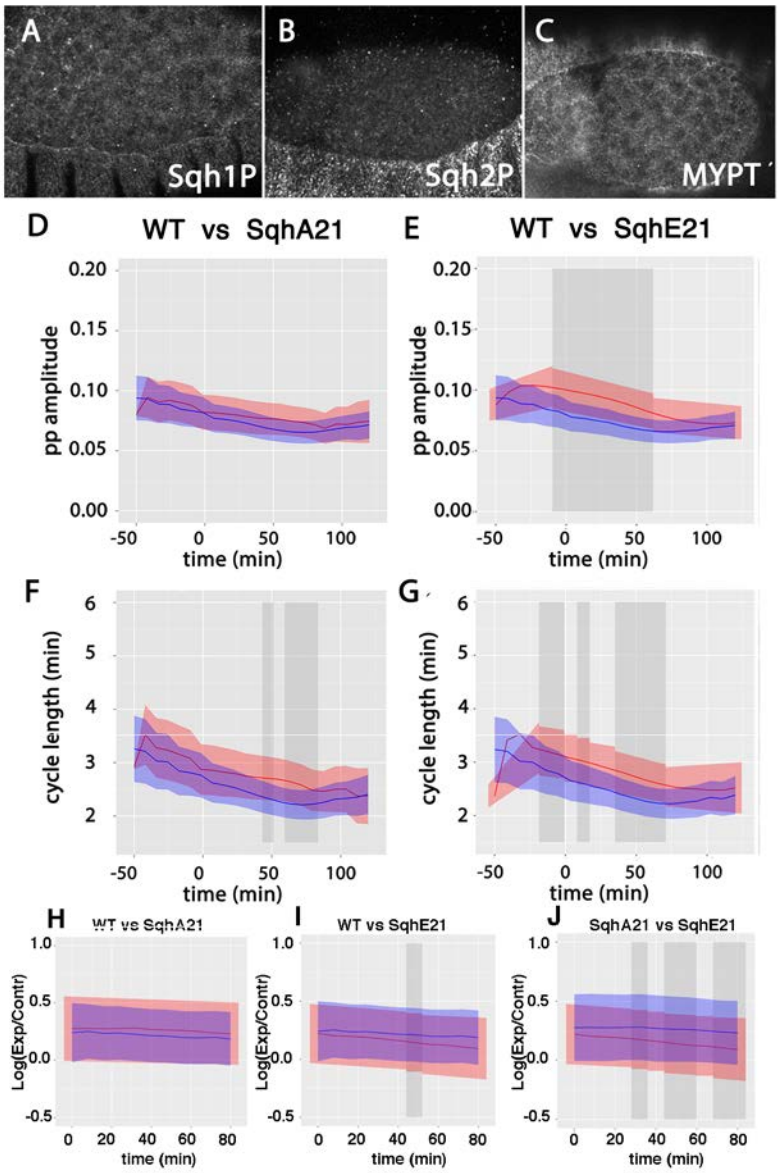

Figure S1. Myosin phosphorylation in amnioserosa cells. (A) Stage 13 embryo stained for an antibody against the monophosphorylated form of Sqh (Sqh1P). (B) Stage 13 embryo stained for an antibody against the diphosphorylated form of Sqh (Sqh2P). (C) Stage 14 embryos stained for an antibody against Mbs (MYPT). (D-J) Statistical analysis of cell shape oscillations. Average amplitude (D, E), average cycle length (F, G) and Log ratio of expansion to contraction (H-J), of AS cell oscillations over time from wild-type (blue) and Sqh phosphomutant (red) embryos. In J, SqhA21 embryos are in blue and SqhE21 embryos are in red. In these and in the following similar plots, the shaded area corresponds to regions of significant differences applying a linear-mixed effect model (see SMM).

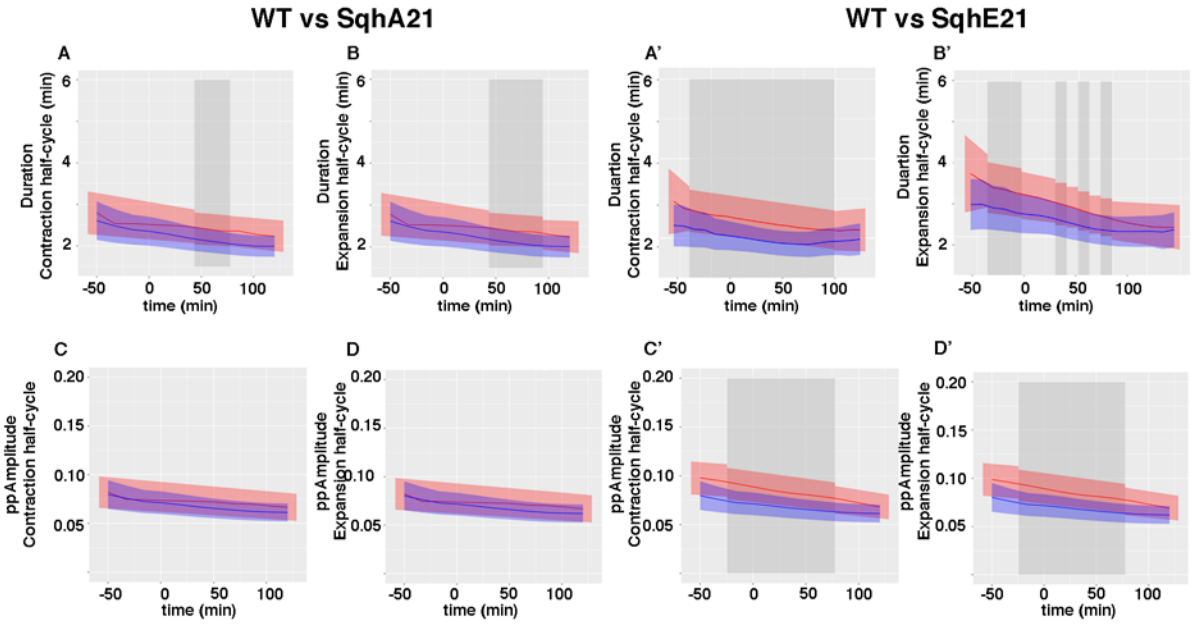

Figure S2. Statistical analysis of the amplitude and period of fluctuation half-cycles. (A-D') Average cycle length (A-B') and average proportional amplitude (C-D') of AS cell contraction (A,A', C,C') and expansion (B,B',D.D') half-cycles over time from wild-type (blue) and Sqh phosphomutant (red) embryos. Note that the cycle length of half-cycles is shown as a full cycle length.

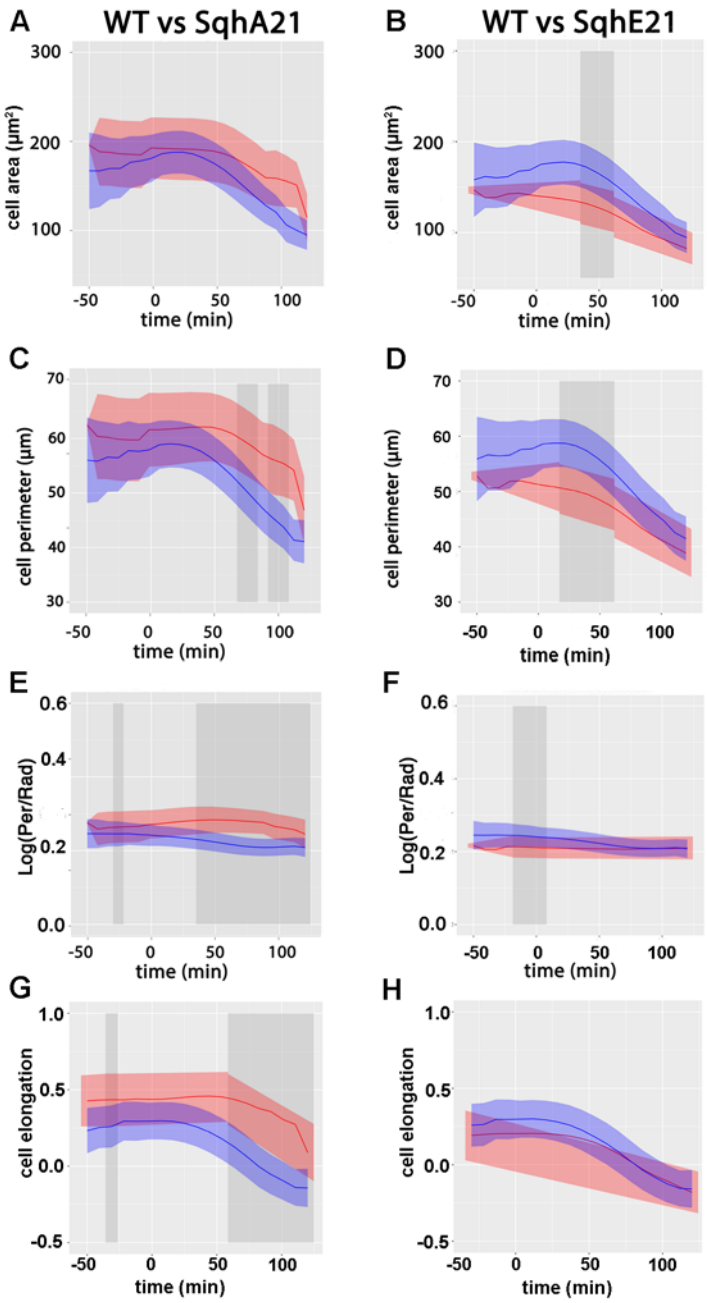

Figure S3. Statistical analysis of cell shape. Average apical cell area (A, B), average cell perimeter (C, D), log ratio of cell perimeter to cell area (E, F) and DV cell elongation (G, H) over time of AS cells from wild-type (blue) and Sqh phosphomutant (red) embryos.

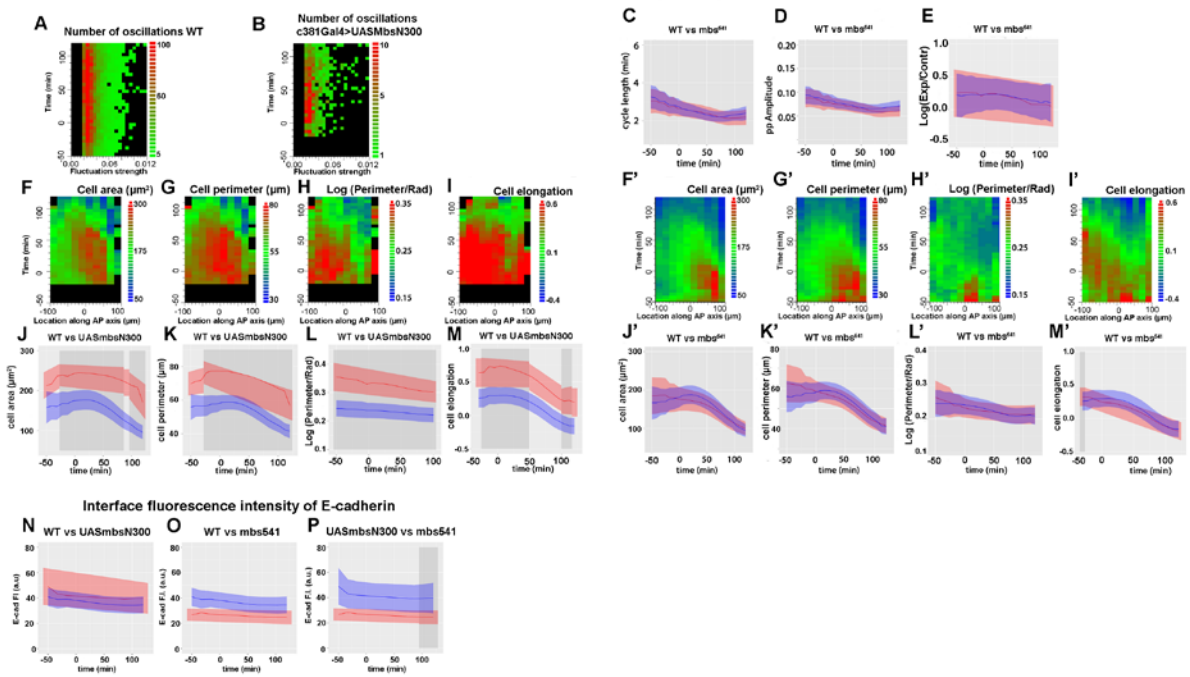

Figure S4. (A-M') Statistical analysis of AS cell oscillations and shape in c381Gal4>UASMbsN300 and *mbs*^{541} embryos. (A, B) Number of valid fluctuation events over time in 7 wild-type (A) and 5 c381Gal4>UASMbsN300 (B) embryos. Note that the colour-code is different, with red representing more than 100 fluctuations events in wild-type embryos and only 10 in c381Gal4>UASMbsN300 embryos. (F-M) Cell shape in c381Gal4>UASMbsN300 embryos. Cell area (F), cell perimeter (G), log ratio of cell perimeter to area (H) and ML cell elongation (I) of AS cells from 5 c381Gal4>UASMbsN300 embryos as a function of their location along the AP axis over time. Statistical analysis of average cell area (J), cell perimeter (K), log ratio of cell perimeter to area (L) and DV cell elongation (M) over time of AS cells from wild-type (blue) and c381Gal4>UASMbsN300 (red) embryos. Average cycle length (C), amplitude (D) and log ratio of expansion to contraction half-cycle durations (E) of AS cell shape oscillations over time from 7 wild-type (blue) and 5 *mbs*^{541} (red) embryos. No significant differences are observed. Cell area (F'), cell perimeter (G'), log-ratio of cell perimeter to area (H') and ML cell elongation (I') of AS cells from five *mbs*^{541} embryos as a function of their location along the AP axis over time. (J'-M') No statistical differences between wild-type and *mbs*^{541} mutant embryos are observed for any of these parameters. (N-P) Statistical analysis of DE-cadherin fluorescence intensity at cell interfaces in 6 wild-type, 5 *mbs*^{541} and 3 c381Gal4>UASMbsN300 embryos. No significant differences are observed between wild-type (blue) and c381Gal4>UASMbsN300 (red) (N), nor between wild-type (blue) and *mbs*^{541} (red) (O) embryos, but we could detect some significant differences between c381Gal4>UASMbsN300 (blue) and *mbs*^{541} (red), at the end of DC (P).

Table S1: Myosin foci dynamics (mean value ± SD).

	UASmbsN300	sqhA21	WT	sqhE21	*mbs*^{541}
Duration of Myosin foci (min)	1.87 ± 0.78	1.57 ± 0.63	1.60 ± 0.52	1.43 ± 0.40	1.37 ± 0.46
Time interval between consecutive foci (min)	1.73 ± 1.71	1.52 ± 1.07	1.28 ± 0.93	0.90 ± 0.76	0.98 ± 0.81
Myosin foci cycle length (min)	3.67 ± 1.90	3.09 ± 1.28	2.82± 1.02	2.35 ± 0.88	2.39 ± 0.92
Persistence of Myosin	0.59 ± 0.22	0.55 ± 0.21	0.61 ± 0.19	0.64 ± 0.19	0.62 ± 0.20

Supplementary Movies

Movie 1. Time-lapse movie of a *sqh*^{1}; sqh-sqhA21::GFP embryo (left), a *sqh*^{1}; sqh-sqh::GFP embryo (centre) and a *sqh*^{1}; sqh-sqhE21::GFP embryo (right). Time interval: 15 seconds.

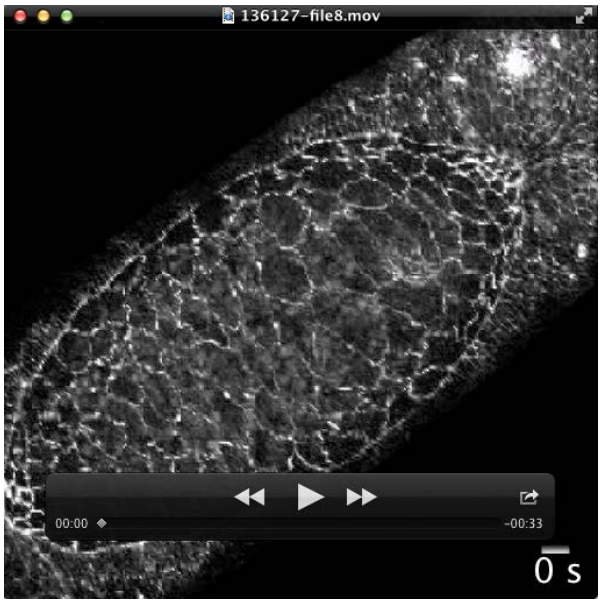

Movie 2. Time-lapse movie of a *sqh*^{1}; sqh-sqhA21, DE-Cadherin::GFP embryo from 20 min. of DC. Time interval: 30 seconds.

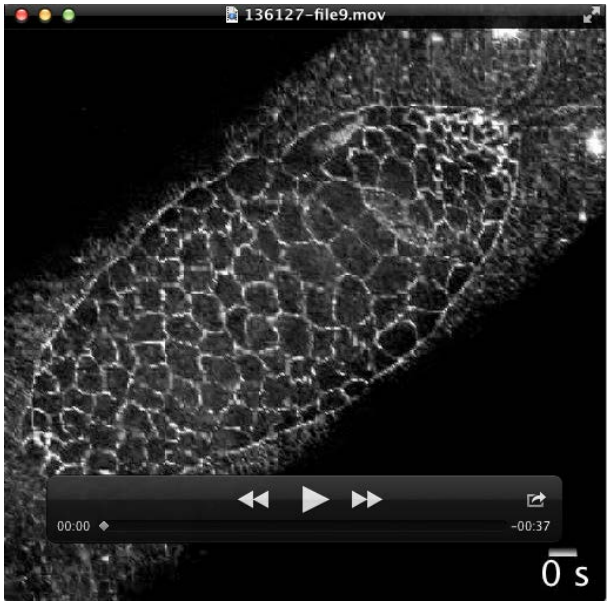

Movie 3. Time-lapse movie of a *sqh*^{1}; sqh-sqhE21, DE-Cadherin::GFP embryo from 20 min. of DC. Time interval: 30 seconds.

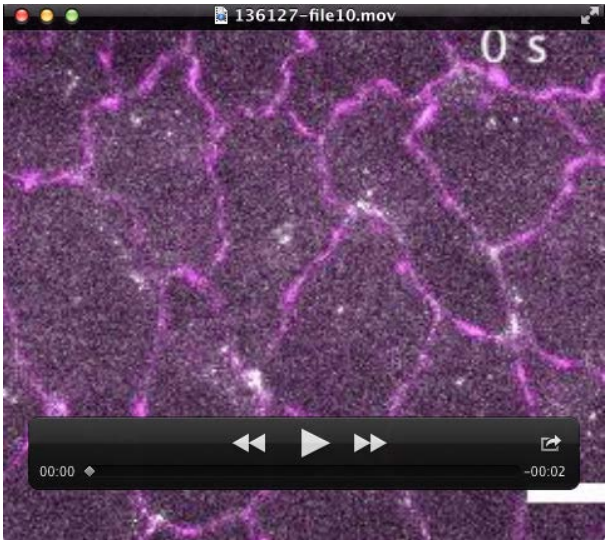

Movie 4. Time-lapse movie of a DE-Cadherin::mTomato/sqh-RokK116A::GFP embryo. Time interval: 30 seconds.

Movie 5: Time-lapse movie of a daGal4>UAS-RokWT::Venus embryo in a *rok*^{2} maternal and zygotic mutant background. Time interval: 30s.

Movie 6: Time-lapse movie of a DE-Cadherin::mTomato, sqh::GFP embryo, a DE-Cadherin::mTomato, sqh::GFP embryo incubated with the Rok inhibitor Y-27632 at 1mM, and a DE-Cadherin::mTomato, sqh-GFP; *mbs*^{541} embryo. Time interval: 15 seconds.

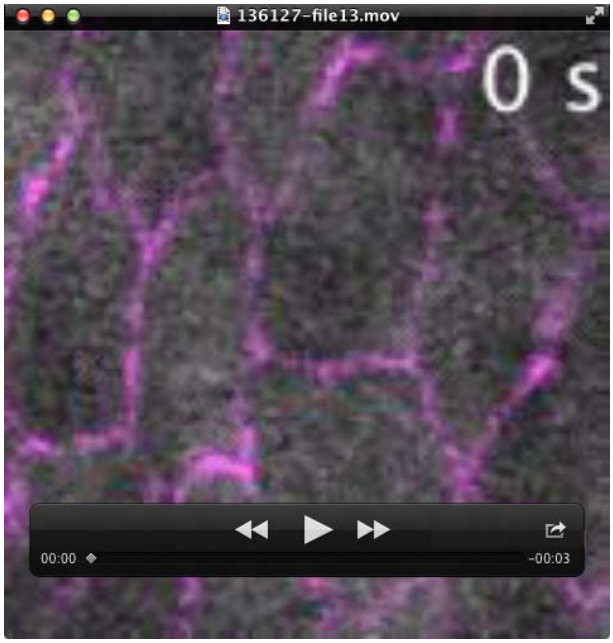

Movie 7. Time-lapse movie of a c381Gal4, DE-Cadherin::mTomato/UAS-Mbs::GFP embryo. Time interval: 30 seconds.

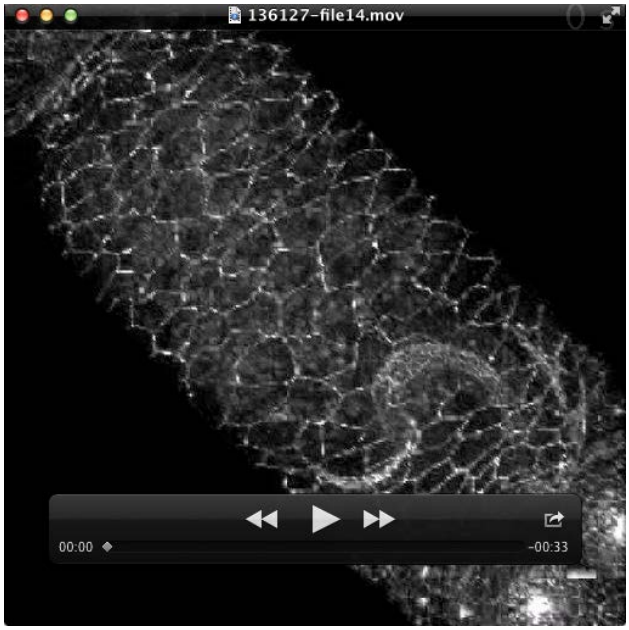

Movie 8. Time-lapse movie of a C381Gal4, DE-cadherin::GFP/UAS-MbsN300 from 20 min. of DC. Time interval: 30s

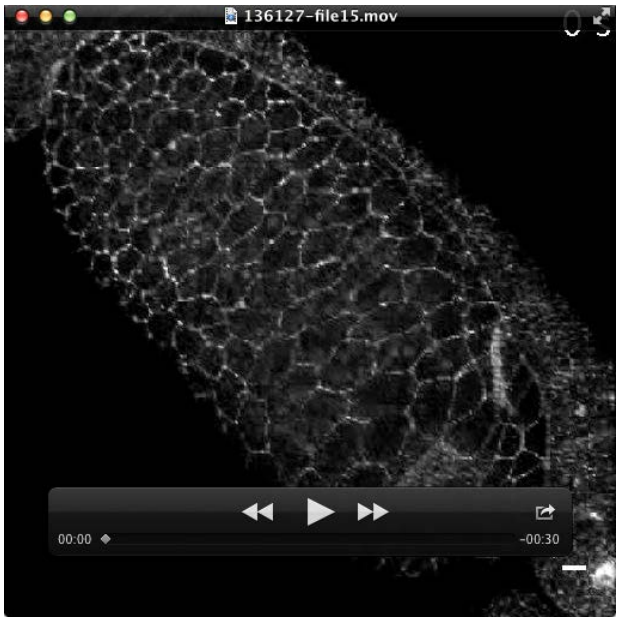

Movie 9. Time-lapse movie of a DE-Cadherin-GFP, *mbs*^{541} embryo from 20 min. of DC. Time interval: 30 seconds.

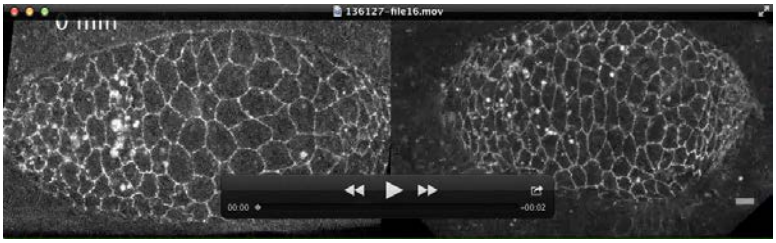

Movie 10. Time-lapse movie of a C381Gal4, DE-Cadherin-mTomato/UAS-MoesinT599A; mbs^{541} embryo and a C381Gal4, DE-Cadherin-mTomato/UAS-MoesinT599D; mbs^{541} embryo. Time interval: 10 minutes.

Supplementary references

Blanchard, G.B., Murugesu, S., Adams, R.J., Martinez-Arias, A., and Gorfinkiel, N. (2010). Cytoskeletal dynamics and supracellular organisation of cell shape fluctuations during dorsal closure. Development (Cambridge, England) *137*, 2743-2752.
Huang, J., Zhou, W., Dong, W., and Hong, Y. (2009). Targeted engineering of the Drosophila genome. Fly (Austin) *3*, 274-277.
Jordan, P., and Karess, R. (1997). Myosin light chain-activating phosphorylation sites are required for oogenesis in Drosophila. The Journal of cell biology *139*, 1805-1819.
Lee, A., and Treisman, J.E. (2004). Excessive Myosin activity in mbs mutants causes photoreceptor movement out of the Drosophila eye disc epithelium. Molecular biology of the cell *15*, 3285-3295.
Oda, H., and Tsukita, S. (2001). Real-time imaging of cell-cell adherens junctions reveals that Drosophila mesoderm invagination begins with two phases of apical constriction of cells. Journal of cell science *114*, 493-501.
Sen, A., Nagy-Zsver-Vadas, Z., and Krahn, M.P. (2012). Drosophila PATJ supports adherens junction stability by modulating Myosin light chain activity. The Journal of cell biology *199*, 685-698.
Speck, O., Hughes, S.C., Noren, N.K., Kulikauskas, R.M., and Fehon, R.G. (2003). Moesin functions antagonistically to the Rho pathway to maintain epithelial integrity. Nature *421*, 83-87.
Vasquez, C.G., Tworoger, M., and Martin, A.C. (2014). Dynamic myosin phosphorylation regulates contractile pulses and tissue integrity during epithelial morphogenesis. The Journal of cell biology *206*, 435-450.